Identifying the Location in the Host Galaxy of Short GRB 111117A with the *Chandra* Sub-arcsecond Position

T. Sakamoto[1,2,3], E. Troja[4], K. Aoki[5], S. Guiriec[4], M. Im[6], G. Leloudas[16,7], D. Malesani[7], A. Melandri[8], A. de Ugarte Postigo[11,7], Y. Urata[9], D. Xu[10], P. D'Avanzo[8], J. Gorosabel[11], Y. Jeon[6], R. Sánchez-Ramírez[11], M. I. Andersen[7,17], J. Bai[19,20], S. D. Barthelmy[3], M. S. Briggs[23], S. Foley[24], A. S. Fruchter[13], J. P. U. Fynbo[7], N. Gehrels[3], K. Huang[12], M. Jang[6], N. Kawai[14], H. Korhonen[17,22], J. Mao[21,19,20], J. P. Norris[15], R. D. Preece[23], J. L. Racusin[3], C. C. Thöne[11], K. Vida[18] X. Zhao[19,20]

ABSTRACT

We present our successful program using *Chandra* for identifying the X-ray afterglow with sub-arcsecond accuracy for the short GRB 111117A discovered by *Swift* and *Fermi*. Thanks to our rapid target of opportunity request, *Chandra* clearly detected the X-ray afterglow, whereas no optical afterglow was found in deep optical observations. Instead, we clearly detect the host galaxy in optical and also in near-infrared bands. We found that the best photometric redshift fitof the host is $z = 1.31^{+0.46}_{-0.23}$ (90% confidence), making it one of the highest redshift short GRBs. Furthermore, we see an offset of 1.0 ± 0.2 arcseconds, which corresponds to 8.4 ± 1.7 kpc assuming z=1.31, between the host and the afterglow position. We discuss the importance of using *Chandra* for obtaining sub-arcsecond localization of the afterglow in X-rays for short GRBs to study GRB environments in great detail.

Subject headings: gamma rays: bursts

[1]Center for Research and Exploration in Space Science and Technology (CRESST), NASA Goddard Space Flight Center, Greenbelt, MD 20771

[2]Joint Center for Astrophysics, University of Maryland, Baltimore County, 1000 Hilltop Circle, Baltimore, MD 21250

[3]NASA Goddard Space Flight Center, Greenbelt, MD 20771

[4]NASA Postdoctoral Program Fellow, Goddard Space Flight Center, Greenbelt, MD 20771

[5]Subaru Telescope, National Astronomical Observatory of Japan, 650 North A'ohoku Place, Hilo, HI 96720

[6]Center for the Exploration of the Origin of the Universe (CEOU), Department of Physics and Astronomy, Seoul National University, Seoul, 151-747, Korea

[7]Dark Cosmology Centre, Niels Bohr Institute, University of Copenhagen, Juliane Maries Vej 30, 2100 Copenhagen Ø, Denmark

[8]INAF - Osservatorio Astronomico di Brera, via Bianchi 46, I-23807 Merate (LC), Italy

[9]Institute of Astornomy, National Central University, Chung-Li 32054, Taiwan

[10]Department of Particle Physics and Astronomy, The Weizmann Institute of Science, Rehovot 76100, Israel

[11]Instituto de Astrofísica de Andalucía (CSIC), Glorieta de la Astronomía s/n, 18008 Granada, Spain

[12]Academia Sinica Institute of Astronomy and Astrophysics, Taipei 106, Taiwan

[13]Space Telescope Science Institute, 3700 San Martin Drive, Baltimore, MD 21218

[14]Department of Physics, Tokyo Institute of Technology, 2-12-1 Ookayama, Meguro-ku, Tokyo 152-8551, Japan

[15]Physics Department, Boise State University, 1910 University Drive, Boise, ID 83725

[16]The Oskar Klein Centre, Department of Physics, Stockholm University, 106 91 Stockholm, Sweden

[17]Niels Bohr Institute, University of Copenhagen, Juliane Maries Vej 30, 2100 Copenhagen, Denmark

[18]Konkoly Observatory of the Hungarian Academy of Sciences, Konkoly Thege út 15-17, 1121, Budapest XII, Hungary

[19]Yunnan Astronomical Observatory, Chinese Academy of Sciences, Kunming, Yunnan Province, 650011, China

[20]Key Laboratory for the Structure and Evolution of Celestial Objects, Chinese Academy of Sciences, Kunming,

1. Introduction

Gamma-ray bursts (GRBs) are traditionally divided in two classes based on their duration and spectral hardness: the long duration/soft spectrum GRBs, and the short duration/hard spectrum GRBs (Kouveliotou et al. 1993). The two classes of bursts further differ in their spectral lags, the measurement of the delay in the arrival time of the low-energy photons with respect to the higher energy ones: long bursts tend to have large positive lags, while short bursts exhibit negligible or negative lags (Norris & Bonnell 2006). The long standing paradigm is that these two phenomenological classes of GRBs originate from different progenitor systems. A preponderance of evidence now links long GRBs with the death of massive stars (Woosley & Bloom 2006, and references therein), yet the origin of short GRBs remains largely unknown. The common notion that short bursts originate from coalescing compact binaries, either neutron star-neutron star (NS-NS) or neutron star-black hole (NS-BH) mergers (e.g., Eichler et al. 1989; Paczynski 1991; Narayan et al. 1992; Rosswog 2005; Rezzolla et al. 2011), makes them the most promising tool to aid in the direct detection of gravitational waves (GWs) by forthcoming facilities such as Advanced-LIGO, Advanced-VIRGO or LCGT (KAGRA) (e.g., Nissanke et al. 2010). It is therefore of primary importance to convincingly corroborate the mergers scenario with a robust observational basis.

Significant progress in understanding the origin of short GRBs has been achieved only recently. This advance was enabled by the detection of their afterglows in 2005 thanks to the rapid position notice and response by *HETE-2* (Ricker et al. 2003) and *Swift* (Gehrels et al. 2004). The first X-ray afterglow of a short GRB was discovered in GRB 050509B by *Swift* (Gehrels et al. 2005; Bloom et al. 2006), allowimg us to localize a short GRB within a $\sim 5''$ accuracy, to identify its host galaxy and therefore determine its redshift. Just two months after this discovery, the first optical afterglow of a short GRB was discovered from GRB 050709 detected by *HETE-2* (Villasenor et al. 2005; Fox et al. 2005; Hjorth et al. 2005). The optical position, which is characterized by a sub-arcsec accuracy, allowed us to unambigously identify the GRB host, but also to precisely pinpoint the GRB location within its galaxy, in a region of low-star formation. The very first localizations of short GRBs immediately provided us with fundamental clues about their nature. They demonstrated that short GRBs are cosmological events with an energy scale of 10^{49}-10^{51} erg, that they occur in a different environment from long GRBs, and are not associated with bright Type Ic supernovae (Bloom et al. 2006; Prochaska et al. 2006; Covino et al. 2006).

Since 2005 the sample of well-localized short GRBs has significantly grown, allowing for a deeper insight into the nature of their progenitors. The observed redshift distribution, ranging $0.11 \lesssim z \lesssim 1$, hints at a progenitor system with a broad range of lifetimes (Berger et al. 2007). This is also consistent with the heterogeneous sample of galaxies harboring short bursts (e.g. Malesani et al. 2007; D'Avanzo et al. 2009; Leibler & Berger 2010). According to Berger (2011), $\sim$50% of short GRBs occur in star forming galaxies, 10% of short GRBs are associated with elliptical galaxies, while the remaining 40% cannot be classified due to various observational constraints. Although a larger fraction of short GRB hosts are star forming galaxies, they differ from star forming host galaxies of long GRBs, which have lower masses and younger population ages (Gorosabel et al. 2006; Leibler & Berger 2010). Another critical test of the progenitor models is the observed offset distribution of short bursts (Troja et al. 2008; Fong et al. 2010; Church et al. 2011). The median physical projected offset between the host center and the short GRB position is $\sim$5 kpc (Fong et al. 2010), which is about five times larger than that of long GRBs (Bloom et al. 2002), and shows a broader dispersion. This is in agreement with the merger scenario, as in several models NS-NS/NS-BH systems are expected to receive significant kick

650011, China

[21]Space Science Division, Korea Astronomy and Space Science Institute, 776, Daedeokdae-ro, Yuseong-gu, Daejeon, 305-348, Republic of Korea

[22]Centre for Star and Planet Formation, Natural History Museum of Denmark, University of Copenhagen, Øster Voldgade 5-7, DK-1350 Denmark

[23]Center for Space Plasma and Aeronomic Research, University of Alabama in Huntsville, 320 Sparkman Drive, Huntsville, AL 35805, USA

[24]Max-Planck-Institut für extraterrestrische Physik, Giessenbachstrasse 1, 85748 Garching, Germany

velocities at birth (Bloom et al. 1999; Fryer et al. 1999; Belczynski et al. 2006), or to dynamically form in globular clusters in the outskirts of their galaxies (Grindlay et al. 2006).

Despite the major progress of the last few years, the study of short GRBs and their progenitors has still been suffering from their less secure afterglow positions and redshifts. Unlike long GRBs, none of the redshifts of short GRBs has been directly measured through afterglow spectroscopy, and only in the case of GRB 060121, a photometric redshift was derived from the afterglow spectral energy distribution (de Ugarte Postigo et al. 2006). This is because the optical afterglows are significantly fainter than those of long GRBs (Nysewander et al. 2009; Kann et al. 2011). Almost all of the redshifts of short GRBs are instead measured from spectroscopic observations of the "associated" host galaxy. The likelihood of a spurious association is small when a sub-arcsec position is available (Cobb et al. 2006). However, if an afterglow is only detected by the *Swift* X-Ray Telescope (XRT; Burrows et al. 2005), a chance alignment becomes more significant due to the larger uncertainty in the localization (2-5″). Unfortunately, the latter scenario represents the majority of cases (∼65%).

A further bias is introduced by the fact that sub-arcsecond positions are mainly derived from optical afterglow detections. In the standard fireball model (Sari et al. 1998), the optical brightness depends sensitively on the density of the circumburst environment. This effect disfavors the accurate localization of short GRBs occurring in the lower-density galaxy halo or even outside their own galaxy, in the intergalactic medium. Such populations of large-offest short GRBs has already been hinted at Bloom et al. (2007) and Troja et al. (2008). However being localized mainly by XRT, their association with the putative host galaxy remain uncertain. Increasing the sample of large-offset short bursts with sub-arcsecond localization is crucial to discriminate whether their progenitors were ejected from their birth site, favoring models which predict NS binaries with large kick velocities and ∼Gyr lifetimes, or they were formed from dynamical interactions in globular clusters (Salvaterra et al. 2010).

In this context, rapid *Chandra* observations of short GRB afterglows represent the critical observational gateway to overcome the current observational limits. Since 80% of the *Swift* short GRBs with prompt slewing are detected in X-rays, and only 40% of them are detected in the optical band, X-ray observations have a higher probability of successfully detecting the afterglow of short GRBs. The superb angular resolution of *Chandra* allows for a sub-arcsecond localization comparable to the optical ones, thus enabling the secure host identification and the precise measurement of the GRB projected offset. Furthermore, because the X-ray afterglow is less subject to density effects, *Chandra* localizations allow us to build a sample of well-localized short GRBs with limited bias. This is the key to distinguish among possible different short GRB populations (Sakamoto & Gehrels 2009), which could arise from a different progenitor and/or environment.

In this paper, we report the first results of our *Chandra* program which led to the accurate localization of GRB 111117A detected by *Swift* and *Fermi*. Our results were leveraged with an intense ground-based follow-up campaign. No optical/infrared counterpart was found, therefore our *Chandra* localization uniquely provides the most accurate sub-arcsecond position. The paper is organized as follows: we report the prompt emission properties in §4, the X-ray afterglow properties in §5.1, the deep optical afterglow limits in §5.2, and the host galaxy properties in §6. We discuss and summarize our result in §7. The quoted errors are at the 90% confidence level for prompt emission and X-ray afterglow data, and at the 68% confidence level for optical and near infrared data unless stated otherwise. The reported optical and near infrared magnitudes are in the Vega system unless stated otherwise. Throughout the paper, we use the cosmological parameters, $\Omega_m = 0.27$, $\Omega_\Lambda = 0.73$ and $H_0 = 71$ km s^{-1} Mpc^{-1}.

2. GRB 111117A

On 2011 November 17 at 12:13:41.921 UT, the Burst Alert Telescope (BAT; Barthelmy et al. 2005a) triggered and localized short GRB 111117A (Mangano et al. 2011). The *Fermi* Gamma-ray Burst Monitor (GBM; Meegan et al. 2009) also detected the burst (Foley et al. 2011). The BAT location derived from the ground analysis was (R.A., Dec.) (J2000) = (00^h 50^m 49.4^s , +23°

00′ 36″) with a 90% error radius of 1.8′. The *Swift* XRT started its observation 76.8 s after the trigger. A fading X-ray source was found at the location of (R.A., Dec.) (J2000) = (00^h 50^m 46.22^s , +23° 00′ 39.2″) with a 90% error radius of 2.1″ (Melandri et al. 2011a). The *Swift* UV-Optical Telescope (UVOT; Roming et al. 2005) began the observations of the field 137 s after the trigger, and no optical afterglow was detected (Oates et al. 2011).

The earliest ground observations of the field were performed by the Gao-Mei-Gu telescope (GMG) at 1.96 hr after the BAT trigger. No afterglow was detected with the exposure time of 600 s within the XRT error circle by GMG in the R band (Zhao et al. 2011). The Nordic Optical Telescope (NOT) observed the field at 8.9 hr after the burst, and found an optical source inside the XRT error circle (Andersen et al. 2011). The optical source was confirmed with a possible extended morphology by the Magellan/Baade telescope (Fong et al. 2011), the Gemini-South telescope (Cucchiara et al. 2011), the GROND telescope (Schmidl et al. 2011), and the Telescopio Nazionale Galileo (TNG; Melandri et al. 2011b). The Gran Telescopio CANARIAS (GTC), the Subaru telescope, the United Kingdom Infrared Telescope (UKIRT) and the Canada-France-Hawai Telescope (CFHT) also collected images of the field.

Based on no clear detection of an optical afterglow of the short GRB 111117A, we triggered our *Chandra* Target of Opportunity (ToO) observation 6 hours after the trigger (Sakamoto et al. 2011b), and the observation started 3 days later. The X-ray afterglow was clearly detected in 20 ks, obtaining a sub-arcsecond position of the afterglow in X-rays (Sakamoto et al. 2011c).

3. Data analysis

HEAsoft version 6.11 and the *Swift* CALDB (version 20090130) were used for the *Swift* BAT data analysis. The XRT data products were obtained from the automated results available from the UK *Swift* Science Data Center (Evans et al. 2007, 2009). CIAO 4.3 and CALDB 4.4.6 were used for the *Chandra* data analysis. The *Fermi* Gamma-ray Burst Monitor (GBM) data were prepared using the RMFIT software package,[1] with data from three Sodium Iodide (NaI) scintillation detectors (detector ID 6, 7 and 9) and two Bismuth Germanate (BGO) scintillation detectors (detector ID 0 and 1).

A standard data reduction of optical and near infrared images was performed using the IRAF[2] software package. The SExtractor[3] (Bertin & Arnouts 1996), the SkyCat GAIA[4] and IRAF were used to extract sources and perform the photometry. To accomplish consistent photometry for images collected by various telescopes, we selected 10 common stars in the field and perform a relative photometry (Table 1). When some of the stars were saturated (especially for a large aperture telescope such as GTC), a subset of these 10 reference stars were used. The USNO B-1 R2 magnitude or the SDSS magnitudes were used as the reference magnitude for the stars. For the near infrared images of UKIRT and CFHT, we use the reference stars in the 2MASS catalog. The galactic extinction has been corrected using E(B-V) = 0.03 mag toward the direction to this burst (Schlegel et al. 1998). The log of optical and near infrared observations presented in this paper is summarized in Table 2.

4. Prompt Emission

The light curve of the prompt emission is composed of two episodes: the first episode shows multiple overlapping pulses with a total duration of 0.3 s, and the second episode is composed of two pulses with a duration of 0.1 s (Figure 1). The duration is T_{90} = 464 ± 54 ms (1 σ error; 15-350 keV) measured by the BAT background-subtracted light curve using the mask modulation (e.g., mask-weighted light curve). This T_{90} duration is significantly shorter than 2 s, which is the standard classification of short GRBs in the BATSE GRBs (Kouveliotou et al. 1993). Furthermore, this duration is shorter than 0.7 s, which is claimed to be the dividing line between long and short GRBs for the *Swift* sample (Bromberg et al. 2012). The hard-to-soft spectral evolution is seen in both the first and the second episodes

[1] http://fermi.gsfc.nasa.gov/ssc/data/analysis/user/

[2] http://iraf.noao.edu/

[3] http://www.astromatic.net/software/sextractor

[4] http://astro.dur.ac.uk/~pdraper/gaia/gaia.html

of GRB 111117A (see the hardness ratio plot at the bottom panel of Figure 1). There is no indication of extended emission (Norris et al. 2011) down to a flux level of $\sim 2 \times 10^{-10}$ erg cm^{-2} s^{-1}, assuming a power-law spectrum with a photon index of -2 in the 14-200 keV band by examining the BAT sky image from 60 s (after the spacecraft slew settled) to 950 s after the BAT trigger time (hereafter $t_{0,\rm BAT}$). The spectral lag between the 100-350 keV and the 25-50 keV band is 0.6 ± 2.4 ms, which is consistent with zero, using the BAT raw light curves (non mask-weighted light curves) by subtracting the background by a constant rate around the burst. In the fluence ratio versus T_{90} plane, GRB 111117A is located in the same region where most of the BAT short GRBs are populated (Figure 2).

The time-integrated spectral properties are investigated by performing a joint spectral analysis with BAT and GBM data. The spectrum is extracted from $t_{0,\rm BAT}$ + 0.024 s to $t_{0,\rm BAT}$ + 0.520 s using `batbinevt` for the BAT data and using the RMFIT software package for the GBM data in the same time interval. The BAT energy response file is generated by `batdrmgen`. The energy response files located at the HEASARC *Fermi* archive for trigger bn111117510 are used for the GBM. We use the `xspec` spectral fitting package to do the joint fit. The energy ranges of 15-150 keV, 8-900 keV and 0.2-45 MeV are used for the BAT, the GBM-NaI and the GBM-BGO instruments, respectively. A constant factor is multiplied by the model to take into account the calibration uncertainty among the different instruments. The best fit spectral parameters are summarized in Table 3. We find that a power-law multiplied by an exponential cutoff (CPL) [5] provides the best representative model of the data. The best fit parameters in this model are the power-law photon index $\alpha^{\rm CPL} = -0.28^{+0.31}_{-0.26}$ and $\rm E_{peak} = 420^{+170}_{-110}$ keV (χ^2/d.o.f. = 627/661). The 90% confidence interval of a constant factor of the GBM detectors is between 0.50 and 0.78 which is an acceptable range taking into account a current spectral calibration uncertainty between the BAT and the GBM. A simple power-law model shows a significantly worse fit to the data (χ^2/d.o.f. = 729/662). There is no significant improvement of χ^2 using a Band function (Band et al. 1993) fit (χ^2/d.o.f. = 627/660) over a CPL fit. A preferential fit to a CPL model and also a systematically harder photon index than that of a long GRB seen in GRB 111117A are general characteristics of a time-integrated spectrum of short GRBs (e.g., Ghirlanda et al. 2009; Ohno et al. 2008). The fluence in the 8-1000 keV band calculated using the best fit time-integrated spectral parameters based on a CPL fit above is $7.3^{+2.6}_{-2.1} \times 10^{-7}$ erg cm^{-2}. Due to a poor statistics to extract a spectrum in a very short time window, a peak flux is calculated by scaling the BAT mask-weighted count-rate into a flux by folding the BAT energy response and assuming the best fit time-integrated spectral parameters in a CPL model. The peak energy flux at the 8-1000 keV band in 50 ms window starting from $t_{0,\rm BAT}$ + 0.450 s is $(3.8 \pm 1.2) \times 10^{-6}$ erg cm^{-2} s^{-1}. The time-resolved spectroscopy is difficult to perform due to the limited statistics in the data.

We search for pre-burst emission analyzing the BAT survey data (Detector Plane Histogram; DPH). Approximately 4.5 hours before the burst trigger, GRB 111117A was in the field of view of BAT (26.1° from the boresight direction) for $\sim$1 ks during the observation of the blazar PKS 0235+16 (observation ID 00030880085). We use `batsurvey` script to process the DPH data. The extracted rates at the location of GRB 111117A are corrected to the on-axis rate by applying an off-axis correction based on observations of the Crab. We find no significant emission during this observation at the location of GRB 111117A. The 3 sigma upper limit assuming a power-law spectrum of a photon index of -2 is 1.4×10^{-9} erg cm^{-2} s^{-1} at the 14-200 keV band in 300 s exposure.

5. Afterglow

5.1. X-rays

The *Swift* XRT X-ray afterglow light curve can be fit to a simple power-law decay (Figure 4). The spectrum collected in the Photon Counting (PC) mode is well described by an absorbed power-law model. The best fit spectral parameters are a photon index of $-2.19^{+0.36}_{-0.38}$ and an excess N_H of

[5] $f(E) \propto E^{\alpha^{\rm CPL}} \exp\left(\frac{-E(2+\alpha^{\rm CPL})}{E_{\rm peak}}\right)$, where $\alpha^{\rm CPL}$ is the power-law photon index and $E_{\rm peak}$ is the peak energy in the νF_ν spectrum.

$1.8^{+1.1}_{-1.0} \times 10^{21}$ cm^{-2} assuming the galactic N_H at the burst direction of 3.7×10^{20} cm^{-2}. Both the measured photon index and N_H of GRB 111117A are consistent with other *Swift* short GRBs.

The *Chandra* observation started at 12:39:25 UT, and ended at 18:39:10 UT on 2011 November 20 with a total exposure of 19.8 ks. The ACIS instrument had five CCD chips (S3, S4, S5, I2 and I3) enabled, with the S3 chip as the aiming point for the source. The data were collected in the FAINT mode. The X-ray afterglow is clearly detected in the *Chandra* observation with 3.9 σ significance by `wavdetect` (source net counts of 8) within the XRT error circle. To refine the astrometry of the *Chandra* data, we apply the same analysis method described in Feng & Kaaret (2008). We extract the *Chandra* image (0.35 - 8 keV) that overlaps with the GTC image ($4.4' \times 8.7'$). The astrometry of the GTC image is calibrated against the SDSS catalog, and its standard deviation is $\sim 0.3''$. We run `wavdetect` with options of scales="1.0 2.0 4.0 8.0 16.0" and sigthresh = 4×10^{-6} to the extracted *Chandra* image. There are four sources which have a good match between the images. Then, we use `geomap` task in the IRAF IMMATCH package to find the best coordinate transformation between the *Chandra* and the GTC image by fitting those four sources. Finally, we apply `geoxytrans` task (IRAF IMMATCH package) for the originally detected *Chandra* position using the coordinate transformation calculated by `geomap` to find the astrometrically corrected *Chandra* afterglow position. The refined afterglow position is shifted δR.A. $= -0.221''$ and δDec. $= -0.020''$ from the position originally derived by `wavdetect`. The best *Chandra* X-ray afterglow position is (R.A., Dec.) (J2000) = ($00^h\ 50^m\ 46.264^s$, $+23°\ 00'\ 39.98''$) with 1 σ statistical uncertainty of $0.09''$ in right ascension and $0.16''$ in declination coordinate. The *Chandra* position is well within the XRT 90% error circle (see Figure 3).

The combined *Swift* XRT and *Chandra* X-ray afterglow light curve is well fit by a simple power-law with the index of $-1.25^{+0.09}_{-0.12}$. As shown in Figure 4, the X-ray afterglow of GRB 111117A belongs to a dim population of the *Swift* short GRBs. When applying the classification scheme of X-ray afterglow of short GRBs suggested by Sakamoto & Gehrels (2009), the afterglow is classified as a "short-lived" X-ray afterglow since the X-ray flux at 10^4 s after the trigger is $< 10^{-13}$ erg cm^{-2} s^{-1}.

5.2. Optical

We investigate the possible optical afterglow emission by using the image subtraction technique between the early and the late time epoch observations by TNG and GTC. We use ISIS software package (Alard & Lupton 1998) to perform the image subtraction. The early and the late epoch observations of TNG and GTC were obtained at $t_{0,\rm BAT}$ + 7.23 hours and $t_{0,\rm BAT}$ + 7.89 hours, and $t_{0,\rm BAT}$ + 11.4 days and $t_{0,\rm BAT}$ + 14.4 days, respectively. We find no significant emission at the *Chandra* X-ray afterglow location in the subtracted images in both the TNG and the GTC observations (Figure 5), with 3 sigma upper limits of $R > 24.1$ mag for TNG and $r > 24.9$ (AB) mag for GTC. The TNG limiting magnitudes of the first and second epochs are $R > 24.7$ mag and $R > 25.4$ mag, respectively. For GTC, the limiting magnitude of the first and second epoch are $r > 25.8$ (AB) mag and $r > 26.1$ (AB) mag, respectively. Those limits are some of the deepest optical limits on short GRBs ever obtained (see upper panel of Figure 6).

6. Host Galaxy

The host galaxy of GRB 111117A has been detected from the near infrared to the optical bands. There is only one near-infrared and optical source located near the *Chandra* X-ray afterglow position. Although the weak nature of the source makes it difficult to investigate whether the source is extended or not, the optical flux of the source is constant between 7 hours and 14 days after the burst at a level of ~ 1.1 μJy (bottom panel of Figure 6). Therefore, we conclude that the source detected in K, J, z, i, r, g, and R bands is the host galaxy of GRB 111117A (Figure 7).

To estimate the redshift of the host galaxy, we perform a spectral energy density (SED) fit with the stellar population model of Maraston (2005). We use the Single Stellar Populations (SSP) models with a Salpeter initial mass function (Salpeter 1955), solar metallicity which ranges from 0.005 $Z_\odot$ to 3.5 $Z_\odot$ (0.005, 0.02, 0.5, 1.0, 2.0 and 3.5 $Z_\odot$), and a red or blue horizontal branch morphology. A total number of 269 SED templates ranging in stellar age from 10 Myr to 15 Gyr was

applied. The Bayesian Photometric Redshift software (BPZ; Benítez 2000) is used to fit the data in g, r, and i bands (GTC), z band (GMG), J band (CFHT) and K band (UKIRT) with those SED templates. We found that the best fit SED template corresponds to a solar metalicity, a red horizontal branch morphology and the luminosity weighted mean stellar age of 0.1 Gyr with a redshift of $1.36^{+0.45}_{-1.18}$. Our best fit SED template of SSP model with a solar metallicity and a red horizontal branch matches well with other short GRB hosts studied by Leibler & Berger (2010). As seen in Figure 9 (top), there is a less significant low redshift solution (z < 0.25) in the estimated redshift. We found that this low redshift solution is coming from the template with the young stellar ages of ~10 Myr. As we will discuss in §7, it is unlikely that the host galaxy has the stellar ages of ~10 Myr. Therefore, to constrain the redshift better, we focus on 41 SED templates of a solar metallicity and a red horizontal branch morphology with stellar age from 20 Myr to 15 Gyr. Figure 8 shows the best fit SED and the photometric data. The GTC spectrum with the exposure time of 4 × 1800 s is also shown in the figure. The signal-to-noise is low, and there are no clear absorption or emission line features in the spectrum. The continuum part of the spectrum is consistent with the best fit SED template. Bottom panel of Figure 9 shows the posterior probability distribution of the estimated redshift for this SED fit. No low redshift solution is evident in the probability distribution. We find the best estimated redshift to be 1.31 (90% confidence interval $1.08 < z_{ph} < 1.77$). The likelihood that the redshift is correct is 80% (reduced χ^2 of the fit is 0.65). The best fit SED template is the case with the luminosity weighted mean stellar age of 0.1 Gyr and a mass of $\sim 1 \times 10^9$ $M_\odot$. To investigate the likelihood of the host being a star-forming galaxy, we also examine the SED templates with an exponentially decaying star formation rate (Maraston 2010), with an e-folding time of 0.1, 1 and 10 Gyr (stellar age ranges from 10 Myr to 15 Gyr). Although our J band data point shows a relatively poor agreement with the best fit template with an e-folding time of 0.1 Gyr and the luminosity weighted mean stellar age of 0.3 Gyr, the fit is still acceptable (reduced $\chi^2 = 0.91$). The best fit redshift in this case is $1.18^{+0.61}_{-0.21}$. The fit becomes worse if the e-folding time gets larger. Therefore, our current data also supports the host galaxy to be ~0.1 Gyr post-starburst galaxy. We also fitted the optical-NIR SED using MAGPHYS package (de Cunha et al. 2008) to check the validity of the fitting result. The MAGPHYS fit includes an extinction parameter as a part of the fit, but performs the fitting at a given redshift. An exponentially decaying star formation rate is assumed. The redshifts were increased by a step of 0.05 from 0.8 to 1.5. We confirm that the returned χ^2 is the least in the range of the z_{phot} from the BPZ, and a moderate extinction of $A_V = 0.2 - 0.5$ mag is found. The best fit solutions give the exponential time scale of about 1.5 Gyr, with the luminosity weighted mean stellar age (in r-band) of a few hunder Myr, the stellar mass of a few times 10^9 $M_\odot$. These output values are consistent with the solutions we got already through during the photometric redshift derivation. In summary, based on various SED template fits, we can conclude the followings about the host galaxy. First, the redshift of the host is ~1.3 regardless of the SED model. Second, the host is either a star-forming galaxy of the luminosity weighted mean stellar age of 0.1 Gyr and a mass of $\sim 1 \times 10^9$ $M_\odot$ or a post-starburst galaxy. Further deep J or Y band data are crucial to pin-down the host properties.

A significant offset between the center of the host galaxy and the X-ray afterglow has been found for GRB 111117A. The center position of the host galaxy has been examined by running SExtractor to the 2nd epoch of the GTC r image which is our highest quality optical image. The best location of the host center is (R.A., Dec.) (J2000) = (00^h 50^m 46.258^s, $+23°$ $00'$ $40.97''$). The position changes less than half a pixel ($< 0.13''$) by changing the detection threshold of SExtractor. Therefore, the projected offset between the center of the host galaxy and the X-ray afterglow is $1.0''$ (δR.A. = $0.083''$ and δDec. = $-0.990''$; see Figure 7). Taking into account the statistical error in the X-ray afterglow position of $0.18''$ and the statistical error of the host center location of $0.13''$, we estimate the offset with its error to be 1.0 ± 0.2 arcseconds, which corresponding to a distance of 8.4 ± 1.7 kpc at a redshift of z = 1.31. This offset is consistent with the median offset of 5 kpc for short GRBs (Fong et al. 2010).

Throughout this section, the association be-

tween the GRB and the galaxy close to the *Chandra* position as the host has been assumed. It is however worth discussing the chance association probabilities. Using the formula provided by Bloom et al. (2002), the probability of finding an unrelated galaxy of the R magnitude of $\sim$23.3 with the distance of 1.0″ is 0.8%. Although this probability is comfortably small, it is non-negligible. Therefore, we would like to note the small possibility of a mis-identification of the host galaxy based on our currently available dataset.

7. Discussion

Our photometric redshift of $1.31^{+0.46}_{-0.23}$ (90% confidence) of the host galaxy is a reasonable estimate for the following reasons. First, by plotting the observed r AB magnitude (r_{AB}) of the host galaxies of short GRBs as a function of redshifts (Berger 2009), we find that the relatively low magnitude of the host galaxy of GRB 111117A, $r_{AB} = 24.20 \pm 0.07$, is located at the redshift range of > 0.5 (Figure 10). Second, we found that the less significant low redshift solution ($z < 0.25$) in the photometric redshift estimation (Figure 9) is coming from the templates with the young stellar ages of $\sim$10 Myr. At z=0.25, if the galaxy is star forming, there would be a chance of seeing emissions of [OII], H-β and [OIII] in the optical spectrum. However, we see none of those lines in the GTC spectrum. Furthermore, $\sim$10 Myr is in general too young for a galaxy, and also is in agreement with the lifespan of a 40 $M_\odot$ star. It is very unlikely that NS-NS merger could happen in a $\sim$10 Myr-old galaxy. Therefore, the low redshift solution for the photometric redshift is unlikely to be the case of GRB 111117A. Therefore, hereafter, we will discuss the rest-frame properties of GRB 111117A using our best photometric redshift of 1.31.

Assuming the redshift of 1.31, the isotropic equivalent γ-ray energy ($E_{\gamma,\rm iso}$) which is integrated from 1 keV to 10 MeV at the rest-frame is $3.4^{+5.7}_{-1.5} \times 10^{51}$ erg. The peak energy at the rest-frame ($E^{\rm src}_{\rm peak}$) is 945^{+455}_{-310} keV. The 90% errors in $E_{\gamma,\rm iso}$ and $E^{\rm src}_{\rm peak}$ are taking into account not only a statistical error but also an uncertainty in the estimated redshift. As shown in Figure 11, $E_{\gamma,\rm iso}$ of GRB 111117A is located at the high end of $E_{\gamma,\rm iso}$ distribution of short GRBs and at the low end of $E_{\gamma,\rm iso}$ distribution of long GRBs. Relatively low $E_{\gamma,\rm iso}$ and high $E^{\rm src}_{\rm peak}$ compared to those of long GRBs make GRB 111117A inconsistent with the $E^{\rm src}_{\rm peak}$-$E_{\gamma,\rm iso}$ (Amati) relation (Amati et al. 2002). This characteristic is consistent with being a short GRB because most of the short GRBs are well known outliers of the Amati relation (Amati 2006; Nava et al. 2012). Recently, Margutti et al. (2012) and Bernardini et al. (2012) found a universal scaling among $E_{\gamma,\rm iso}$, $E^{\rm src}_{\rm peak}$ and the X-ray energy emitted in the 0.3-10 keV band ($E_{X,\rm iso}$). This three-parameter relation, the $E_{X,\rm iso}$-$E_{\gamma,\rm iso}$-$E^{\rm src}_{\rm peak}$ relation, is claimed to hold not only for long and short GRBs, but also for low luminosity GRBs. The best fit function is $\log(E_{X,\rm iso}) = 1.06\log(E_{\gamma,\rm iso}) - 0.74\log(E^{\rm src}_{\rm peak}) - 2.36$, with the intrinsic scatter of 0.31 ($1\ \sigma$). It is interesting to see whether GRB 111117A is consistent with the $E_{X,\rm iso}$-$E_{\gamma,\rm iso}$-$E^{\rm src}_{\rm peak}$ relation or not. By integrating the best fit power-law function of the X-ray light curve data of XRT and *Chandra* from the start time ($t_{0,\rm BAT}$ + 90 s) to the end time ($t_{0,\rm BAT}$ + 282 ks), the X-ray fluence in the 0.3-10 keV band is estimated to be 2.3×10^{-8} erg cm^{-2}. Using the redshift of 1.31, $E_{X,\rm iso}$ of GRB 111117A is calculated to be 1.0×10^{50} erg. Therefore, GRB 111117A is located well within 2-σ region from the best fit $E_{X,\rm iso}$-$E_{\gamma,\rm iso}$-$E^{\rm src}_{\rm peak}$ relation. Furthermore, GRB 111117A is populated at the same region where seven short GRBs are located in the $E_{X,\rm iso}$-$E_{\gamma,\rm iso}$-$E^{\rm src}_{\rm peak}$ relation (see Figure 20 of Margutti et al. 2012).

The upper limit on the afterglow emission in optical and the weak X-ray afterglow emission are consistent with a standard afterglow model if a cooling frequency (ν_c) is located above both the optical and the X-ray band with a relatively shallow power-law index (p) for the electron distribution ($p \lesssim 2.1$). The optical-to-X-ray spectral index (Jakobsson et al. 2004), $\beta_{\rm OX}$ ($\equiv \log\{f_\nu(R)/f_\nu(3\,{\rm keV})\}/\log(\nu_{3\,\rm keV}/\nu_{\rm R})$), is estimated to be $\lesssim 0.78$ using the same definition on the X-ray flux density measured at 11 hours after the burst at 3 keV, and the optical afterglow limit based on the GTC r band. This upper limit of $\beta_{\rm OX}$ is within the allowed range of the standard afterglow model between 0.5 to 1.25. Following the discussion on Nysewander et al. (2009), we calculate the flux ratio between the optical (F_R) and the X-ray (F_X) to constrain the stan-

dard afterglow emission model. The flux ratio of GRB 111117A is estimated to be $F_R/F_X \lesssim 590$ using the X-ray flux at 11 hours after the burst at 5 keV, which is the same definition of Nysewander et al. (2009), and the upper limit in r band of GTC. If a cooling frequency is above the optical and the X-ray range ($\nu_c > \nu_X > \nu_R$), the ratio is expressed as $F_R/F_X = (\nu_X/\nu_R)^{(p-1)/2}$. Based on our upper limits on the ratio, the power-law index of the electrons has to be $\lesssim 2.7$ to be consistent with a standard afterglow model. On the other hand, the case where the cooling frequency is below the optical band ($\nu_c < \nu_R < \nu_X$), the ratio is expressed as $F_R/F_X = (\nu_X/\nu_R)^{p/2}$. When we apply the constraint in the ratio of $F_R/F_X \lesssim 590$, we find that p has to be smaller than 1.7.

If the cooling frequency is between the optical and the X-ray bands ($\nu_R < \nu_c < \nu_X$), we can put a constraint on the density of the circumburst medium (n_0). In this situation, the flux ratio is expressed as,

$$F_R/F_X = 14.3\,(\nu_X/\nu_R)^{(p-1)/2}(1+z)^{1/4}E_{52}^{1/4}\epsilon_{B,-2}^{3/4}n_0^{1/2},$$

where $\epsilon_{B,-2}$ is the fraction of energy that goes into the electrons in units of 10^{-2} and E_{52} is the energy in units of 10^{52} erg (Nysewander et al. 2009). Applying the flux ratio limit of $F_R/F_X \lesssim 590$ and also assuming $\epsilon_B \approx 0.01$, $E \approx E_{\gamma,\rm iso}$ and $p = 2.1$, n_0 can be constrained as $n_0 \lesssim 0.3$ cm^{-3}. For $p = 2.5$, we find $n_0 \lesssim 0.01$ cm^{-3}. Therefore, we find a significantly smaller n_0 compared to that of a typical value for long GRBs of $n_0 \approx 1-10$ cm^{-3} (e.g., Soderberg et al. 2006), which is likely to be required to explain our optical afterglow limit for GRB 111117A. This finding is consistent with several other short GRBs with no optical afterglow detection (Berger 2010).

We have discussed the optical afterglow limit based on the external shock model. However, there is a possibility that a significant amount of the optical afterglow flux was extinguished by the host galaxy. When we fit the X-ray afterglow spectrum to a power-law model with the intrinsic absorption at z=1.31, the intrinsic N_H is estimated to be $7.2^{+0.7}_{-0.5} \times 10^{21}$ cm^{-2}. A significance of the N_H detection is greater than 2 σ but less than 3 σ confidence level. Assuming a host extinction law similar to the Milky Way galaxy, A_V is 4.1 mag (Predehl & Schmitt 1995). Therefore, a significant amount of absorption in optical flux is expected from the X-ray column density measurement. On the other hand, it is still not clear whether it is possible to have such high extinction at the outskirts of the host where the X-ray afterglow is indicated. Moreover, the amount of extinction which we derived from the SED fit of the host is $A_V = 0.2-0.5$ mag (see §6). At this stage, the origin of the large column density seen in the X-ray afterglow of GRB 111117A is still puzzling. Further deep optical and/or infrared imaging or spectroscopic observation of the host is required to understand the GRB environment.

The projected offset between the afterglow location and the host galaxy center is 8.4 ± 1.7 kpc using the estimated redshift of 1.31. Although this offset is larger than the median projected offset of about 5 kpc for previously studied short GRBs (Fong et al. 2010), it is within the offset distribution of short GRBs. Using the projected offset of $r = 8.4$ kpc and the stellar age of $\tau = 0.1$ Gyr, the minimum kick velocity, $v = r/\tau$, is estimated to be ≈ 80 km s^{-1}. The estimated kick velocity is similar to or possibly larger than the inferred kick velocity of GRB 060502B (Bloom et al. 2007). Using the typical age of 1-10 Gyr in the early-type short GRB hosts such as GRB 050509B, GRB 070809 and GRB 090515 (Bloom et al. 2006; Berger 2010), the minimum kick velocity is estimated to be $\approx$ 1-8 km s^{-1}.

In this paper, we have reported the prompt emission, the afterglow and the host galaxy properties of short GRB 111117A. The prompt emission observed by the *Swift* BAT and the *Fermi* GBM showed 1) a short duration, 2) no extended emission, 3) no measurable spectral lag and 4) a hard spectrum. All those properties can securely classify this burst as a short GRB. Although the optical afterglow has not been detected by our deep observations by TNG and GTC, our rapid *Chandra* ToO observation provides a sub-arcsec position of the afterglow in X-rays. This *Chandra* position is crucial to identify the host galaxy and also to measure the significant offset of 1.0″ between the host center and the afterglow location. Our deep near infrared to optical photometry data of GMG, TNG, NOT, GTC, UKIRT and CFHT enable us to estimate the redshift of the host to 1.31. The observation of GRB 111117A suggests that X-rays are more promising than optical to locate short GRBs with sub-arcsecond accuracy.

Combining the sub-arcsecond afterglow position in the X-ray and the deep optical images from the ground telescopes, we successfully investigate the host properties of GRB 111117A deeply even without an optical afterglow. Rapid *Chandra* ToO observations of short GRBs are still key to increasing the *golden* sample of short GRBs with redshift to pin-down their nature.

This work made use of data supplied by the UK Swift Science Data Centre at the University of Leicester. This work is based on the observations using the United Kingdom Infrared Telescope, which is operated by the Joint Astronomy Centre on behalf of the Science and Technology Facilities Council of the U.K. with a partial support by *Swift* mission (e.g., *Swift* Cycle 7 GI grant NNX12AE75G) and the Gran Telescopio Canarias (GTC), instaled in the Spanish Observatorio del Roque de los Muchachos of the Instituto de Astrofísica de Canarias, in the island of La Palma. The Dark Cosmology Centre is funded by the Danish National Research Fundation. Partly based on observations made with the Nordic Optical Telescope, operated on the island of La Palma jointly by Denmark, Finland, Iceland, Norway, and Sweden, in the Spanish Observatorio del Roque de los Muchachos of the Instituto de Astrofísica de Canarias. This work was supported by *Chandra* Cycle 13 grant GO2-13084X. The research activity of AdUP, CCT, RS-Rand JG is supported by Spanish research projects AYA2011-24780/ESP, AYA2009-14000-C03-01/ESP and AYA2010-21887-C04-01. GL is supported by the Swedish Research Council through grant No. 623-2011-7117. KV is grateful to the Hungarian Science Research Program (OTKA) for support under the grant K-81421. This work is supported by the "Lendület" Young Researchers' Program of the Hungarian Academy of Sciences. HK acknowledges the support from the European Commission under the Marie Curie IEF Programme in FP7. MI and YJ were supported by the he Creative Research Initiative program, No. 2010-0000712, of the National Research Foundation of Korea (NRFK) funded by the Korea government (MEST).

REFERENCES

Ackermann, M., Asano, K., Atwood, W. B., et al. 2010, ApJ, 716, 1178

Akerlof, C. W., Zheng, W., Pandey, S. B., McKay, T. A., 2011, ApJ, 726, 22

Alard, C., Lupton, R. H. 1998, ApJ, 503, 325

Amati, L., Frontera, F., Tavani, M., et al. 2002, A&A, 390, 81

Amati, L. 2006, MNRAS, 372, 233

Andersen, M.I., et al. 2011, GCN Circ. 12563, http://gcn.gsfc.nasa.gov/gcn3/12563.gcn3

Band, D. L., Matteson, J., Ford, L., et al. 1993, ApJ, 413, 281

Barthelmy, S. D., Barbier, L. M., Cummings, J. R., et al. 2005a, Space Sci. Rev., 120, 143

Barthelmy, S. D., Chincarini, G., Burrows, D. N., et al. 2005b, Nature, 438, 994

Belczynski, K., Perna, R., Bulik, T., et al. 2006, ApJ, 648, 1110

Benítez, N. 2000, ApJ, 536, 571

Berger, E., Fox, D. B., Price, P. A., et al. 2007, ApJ, 664, 1000

Berger, E. 2009, ApJ, 690, 231

Berger, E. 2010, ApJ, 722, 1946

Berger, E. 2011, New Astronomy Reviews, 55, 1

Bernardini, M. G., Margutti, R., Zaninoni, E., Chincarini, G. 2012, submitted to MNRAS (arXiv:1203.1060)

Bertin, E., Arnouts, S. 1996, A&AS, 117 393

Bloom, J. S., Sigurdsson, S., Pols, O.R. 1999, MNRAS, 305, 763

Bloom, J. S., Kulkarni, S. R., Djorgovski, S. G. 2002, AJ, 123, 1111

Bloom, J. S., Prochaska, J. X., Pooley, D., et al. 2006, ApJ, 638, 354

Bloom, J. S., Perley, D. A., Chen, H.-W., et al. 2007, ApJ, 654, 878

Bromberg, O., Nakar, E., Piran, T., Sari, R. 2012, ApJ, 749, 110

Burrows, S. D., Hill, J. E., Nousek, J. A., et al. 2005, Space Sci. Rev., 120, 165

Church, R. P., Levan, A. J., Davies, M. B., & Tanvir, N. 2011, MNRAS, 413, 2004

Cobb, B. E., Bailyn, C. D., van Dokkum, P. G., & Natarajan, P. 2006, ApJL, 651, L85

Covino, S., Malesani, D., Israel, G. L., et al. 2006, A&A, 447, L5

Cucchiara, A., et al. 2011, GCN Circ. 12567, http://gcn.gsfc.nasa.gov/gcn3/12567.gcn3

D'Avanzo, P., Malesani, D., Covino, S., et al. 2009, A&A, 498, 711

de Cunha, E., Charlot, S., Elbaz, D., 2008, MNRAS, 388, 1595

de Ugarte Postigo, A., Castro-Tirado, A. J., Guziy, S., et al. 2006, ApJ, 648, L83

Eichler, D., Livio, M., Piran, T., Schramm, D. M., 1989, Nature, 340, 126

Evans, P. A., Beardmore, A. P., Page, K. L., et al. 2007, A&A, 469, 379

Evans, P. A., Beardmore, A. P., Page, K. L., et al. 2009, MNRAS, 397, 1177

Feng, H., Kaaret, P. 2008, ApJ, 675, 1067

Foley, S., et al. 2011, GCN Circ. 12573, http://gcn.gsfc.nasa.gov/gcn3/12573.gcn3

Fong, W., Berger, E., Fox, D. B. 2010, ApJ, 708, 9

Fong, W., et al. 2011, GCN Circ. 12566, http://gcn.gsfc.nasa.gov/gcn3/12566.gcn3

Fox, D. B., Frail, D. A., Price, P. A., et al. 2005, Nature, 437, 845

Fruchter, A. S., Levan, A. J., Strolger, L., et al. 2006, Nature, 441, 4632

Fryer, C. L., Woosley, S. E., Hartmann, D. H. 1999, ApJ, 526, 152

Gehrels, N., Chincarini, G., Giommi, P., et al. 2004, ApJ, 611, 1005

Gehrels, N., Sarazin, C. L. O'Brien, P. T., et al. 2005, Nature, 437, 851

Ghirlanda, G., Nava, L., Ghisellini, G., Celotti, A., Firmani, C. 2009, A&A, 496, 585

Gorosabel, J., Castro-Tirado, A. J., Guziy, S., et al. 2006, A&A, 450, 87

Grindlay, J., Portegies Zwart, S., & McMillan, S. 2006, Nature Physics, 2, 116

Hjorth, J., Watson, D. Fynbo, P. U., et al. 2005, Nature, 437, 859

Jakobsson, P., Hjorth, J., Fynbo, P. U., et al. 2004, ApJ, 617, L21

Kann, D. A., Klose, S., Zhang, B., et al. 2011, ApJ, 734, 96

Kouveliotou, C., Meegan, C. A., Fishman, G. J., et al. 1993, ApJ, 413, L101

Leibler, C. N., Berger, E. 2010, ApJ, 725, 1202

Malesani, D., Covino, S., D'Avanzo, P., et al. 2007, A&A, 473, 77

Mangano, V., et al. 2011, GCN Circ. 12559, http://gcn.gsfc.nasa.gov/gcn3/12559.gcn3

Maraston, C. 2005, MNRAS, 362 799

Maraston, C., Pforr, J., Renzini, A., et al. 2010, MNRAS, 407, 830

Margutti, R., Zaninoni, E., Bernardini, M. G., et al. 2012, submitted to MNRAS (arXiv:1203.1059)

Meegan, C. A., Pendleton, G. N., Briggs, M. S., et al. 1996, ApJS, 106, 65

Meegan, C. A., Giselher, L., Bhat, P. N., et al. 2009, ApJ, 702, 791

Melandri, A., et al. 2011a, GCN Circ. 12565, http://gcn.gsfc.nasa.gov/gcn3/12565.gcn3

Melandri, A., et al. 2011b, GCN Circ. 12570, http://gcn.gsfc.nasa.gov/gcn3/12570.gcn3

Narayan, R., Paczynski, B., Piran, T., 1992, ApJ, 395, L83

Nava, L., Salvaterra, R., Ghirlanda, G., et al. 2012, MNRAS, 421, 1256

Nissanke, S., Holz, D. E., Hughes, S. A., et al. 2010, ApJ, 725, 496

Nysewander, M., Fruchter, A. S., Pe'er, A. 2009, ApJ, 701, 824

Norris, J. P., Bonnell, J. T. 2006, ApJ, 643, 266

Norris, J. P., Gehrels, N., Scargle, J. D. 2011, ApJ, 735, 23

Oates, S. R., et al. 2011, GCN Circ. 12569, 12565, http://gcn.gsfc.nasa.gov/gcn3/12569.gcn3

Ohno, M., Fukazawa, Y., Takahashi, T., et al. 2008, PASJ, 60, 361

Paczynski, B. 1991, Acta Astron., 41, 257

Predehl, P., Schmitt, J. H. M. M, A&A, 293, 889

Prochaska, J. X., Bloom, J. S., Chen, H.-W., et al. 2006, ApJ, 642, 989

Rezzolla, L., Giacomazzo, B., Baiotti, L., et al. 2011, ApJL, 732, L6

Ricker, G. R., Atteia, J.-L., Crew, G. B., et al. 2003, in AIP Conf. Proc. 662, Gamma-Ray Burst and Afterglow Astronomy 2001, ed. G.R.Ricker & R.K. Vanderspek (New York: AIP), 3

Roming, P. W. A., Kennedy, T. E., Mason, K. O., et al. 2005, Space Sci. Rev., 120, 95

Rosswog, S. 2005, ApJ, 634, 1202

Sakamoto, T., Gehrels, N. 2009, in AIP Conf. Proc. 1133, Gamma-Ray Bursts, 6th Huntsville Symposium, ed. C. Meegan, N. Gehrels & C. Kouveliotou (Melville, New York), 112

Sakamoto, T., et al. 2011a, ApJS, 195, 2

Sakamoto, T., et al. 2011b, GCN Circ. 12562, http://gcn.gsfc.nasa.gov/gcn3/12562.gcn3

Sakamoto, T., et al. 2011c, GCN Circ. 12580, http://gcn.gsfc.nasa.gov/gcn3/12580.gcn3

Salpeter, E. E., 1955, ApJ, 121, 161

Salvaterra, R., Devecchi, B., Colpi, M., & D'Avanzo, P. 2010, MNRAS, 406, 1248

Sari, R., Piran, T., & Narayan, R. 1998, ApJL, 497, L17

Schlegel, D. J., Finkbeiner, D. P., Davis, M. 1998, ApJ, 500, 525

Soderberg, A. M., Berger, E., Kasliwal, M., et al. 2006, ApJ, 650, 261

Schmidl, S., et al. 2011, GCN Circ. 12568, http://gcn.gsfc.nasa.gov/gcn3/12568.gcn3

Troja, E., King, A. R., O'Brien, P. T., Lyons, N., & Cusumano, G. 2008, MNRAS, 385, L10

Villasenor, J. S., Lamb, D. Q., Ricker, G. R., et al. 2005, Nature, 437, 855

Woosley, S. E., & Bloom, J. S. 2006, ARA&A, 44, 507

Zhao, X.-H. et al. 2011, GCN Circ. 12560, http://gcn.gsfc.nasa.gov/gcn3/12560.gcn3

Zhang, B., Zhang, B.-B., Virgili, F. J., et al. 2009, 703, 1696

Zheng, W., Akerlof, C.W., Pandey, S.B. et al. 2012, submitted to ApJ (arXiv:1203.5113)

This 2-column preprint was prepared with the AAS LaTeX macros v5.2.

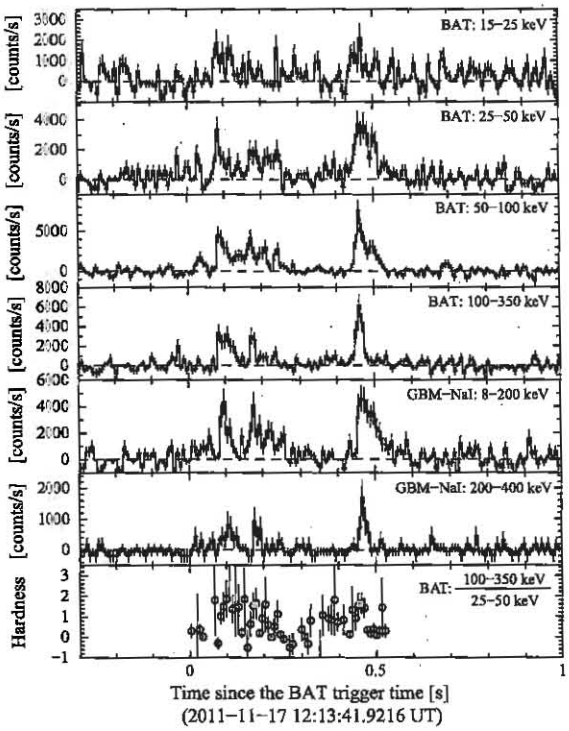

Fig. 1.— The background subtracted 5 ms light curves of *Swift* BAT (15-25 keV, 25-50 keV, 50-100 keV and 100-350 keV) and *Fermi* GBM (8-200 keV and 200-400 keV). The bottom panel shows the hardness ratio between the 100-350 keV and the 25-50 keV of the BAT data.

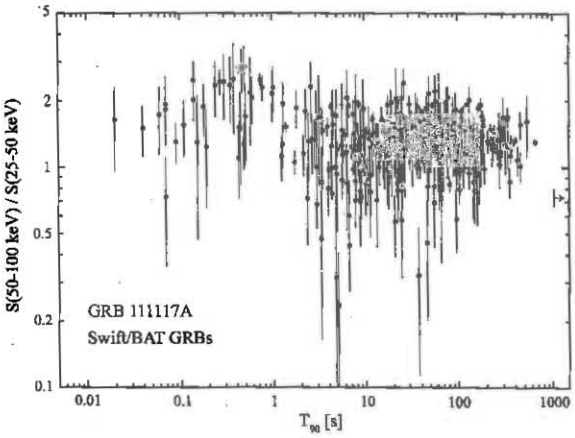

Fig. 2.— Fluence ratios between the 50-100 keV and the 25-50 keV band versus T_{90} are shown for GRB 111117A (red) and the *Swift* BAT GRBs. The values of the *Swift* BAT GRBs are extracted from Sakamoto et al. (2011a).

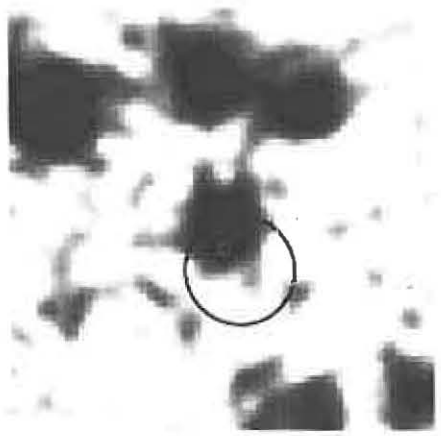

Fig. 3.— GTC r image ($17'' \times 17''$) with the XRT 90% error circle in blue and the *Chandra* 1 sigma error circle in red.

TABLE 1

LIST OF REFERENCE STARS.

R.A. (J2000)	Dec. (J2000)	R2 [mag]	ID of USNO-B1
00:50:45.254	+23:00:59.43	19.76	1130-0013893
00:50:46.923	+23:01:47.81	18.66	1130-0013901
00:50:52.923	+23:01:19.35	16.43	1130-0013919
00:50:36.987	+23:01:25.94	18.58	1130-0013859
00:50:43.442	+22:59:06.91	17.16	1129-0013362
00:50:48.207	+23:00:36.76	15.90	1130-0013906
00:50:41.781	+22:59:33.17	16.78	1129-0013356
00:50:31.795	+22:01:36.78	18.74	1130-0013838
00:50:40.927	+23:02:53.55	16.41	1130-0013875
00:50:51.577	+23:03:10.27	15.42	1130-0013916

TABLE 2

LOG OF OPTICAL AND NEAR-INFRARED OBSERVATIONS OF GRB 111117A. THE MAGNITUDES ARE CORRECTED FOR GALACTIC EXTINCTION.

Time since the trigger* (day)	Telescope	Instrument	Filter	Exposure (s)	Afterglow* (mag)	Host* (mag)
0.083	GMG	YFOSC YSU	R	600		> 22.1
0.104	GMG	YFOSC YSU	z	900		22.9 ± 0.3 (AB)$^\diamond$
0.300	TNG	LRS	R	1800	> 24.1	23.49 ± 0.29
0.329	GTC	OSIRIS	g	800		24.05 ± 0.14 (AB)
0.342	GTC	OSIRIS	r	1200	> 24.9 (AB)	24.17 ± 0.10 (AB)
0.354	GTC	OSIRIS	i	360		23.92 ± 0.20 (AB)
0.358	NOT	ALFOSC	z	3600		> 22.5 (AB)
0.371	NOT	ALFOSC	R	3000		23.20 ± 0.25
1.5	NOT	ALFOSC	R	2400		23.26 ± 0.22
11.4	TNG	LRS	R	3600		23.43 ± 0.13
11.8	Subaru	IRCS	K'	780		> 19.95
14.4	GTC	OSIRIS	r	2400		24.20 ± 0.07 (AB)
$19 - 72^\dagger$	UKIRT	WFCAM	K	8640		20.91 ± 0.12
42.7	CFHT	WIRCam	J	4140		21.7 ± 0.2

*The mean time of the stacked observations with the corresponding exposure time.

†UKIRT data were collected at the multiple epochs between 19 and 72 days after the burst.

*Upper limit is in 3 sigma confidence level.

◇Possible host detection.

TABLE 3
TIME-INTEGRATED SPECTRAL PARAMETERS OF GRB 111117A.

Instrument	Model	α	β	$E_{\rm peak}^{\rm obs}$	C(GBM)	χ^2/dof
BAT	PL	$-0.52^{+0.24}_{-0.22}$	–	–	–	49.5/57 (0.87)
GBM	PL	$-1.44^{+0.06}_{-0.08}$	–	–	–	636.8/604 (1.05)
GBM	CPL	$-0.39^{+0.53}_{-0.37}$	–	440^{+240}_{-125}	–	578.9/603 (0.96)
GBM	Band	$-0.40^{+0.36}_{-0.50}$	<-2.6	450^{+240}_{-125}	–	578.9/602 (0.96)
BAT-GBM	PL	$-1.37^{+0.05}_{-0.07}$	–	–	–	729.5/662 (1.10)
BAT-GBM	CPL	$-0.28^{+0.31}_{-0.26}$	–	420^{+170}_{-110}	$0.62^{+0.16}_{-0.13}$	627.7/661 (0.95)
BAT-GBM	Band	$-0.28^{+0.15}_{-0.26}$	<-2.5	420^{+170}_{-80}	$0.62^{+0.16}_{-0.13}$	627.8/660 (0.95)

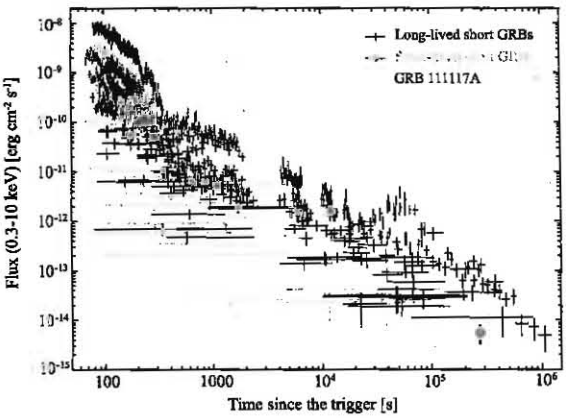

Fig. 4.— Comparison of X-ray afterglow light curves of long-lived and short-lived short GRBs observed by *Swift* XRT and GRB 111117A (red). The *Chandra* data point of GRB 111117A is shown in red filled circle. The long-lived short GRBs include in this figure are GRB 050724, GRB 051221A, GRB 051227, GRB 060313, GRB 061006, GRB 061201, GRB 061210, GRB 070714B, GRB 070724A, GRB 070809, GRB 071227, GRB 080123, GRB 080426, GRB 090426, GRB 090510, GRB 090607, GRB 090621B and GRB 091109B. The short-lived short GRBs include in this figure are GRB 050509B, GRB 050813, GRB 051210, GRB 060502B, GRB 060801, GRB 061217, GRB 070429B, GRB 080503, GRB 080702A, GRB 080905A, GRB 080919, GRB 081024A and GRB 081226A.

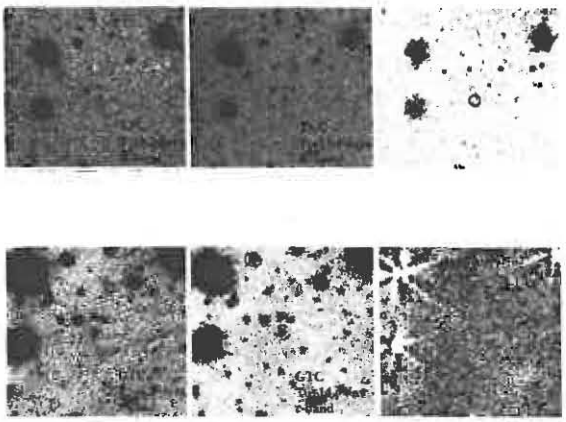

Fig. 5.— Deep optical TNG (R; $1.4' \times 1.2'$) and GTC (r; $1.1' \times 1.0'$) images of two epochs. The right panel shows the subtracted image of the first and second epoch. No significant residuals are seen in both TNG and GTC subtracted images at the host location (red circle).

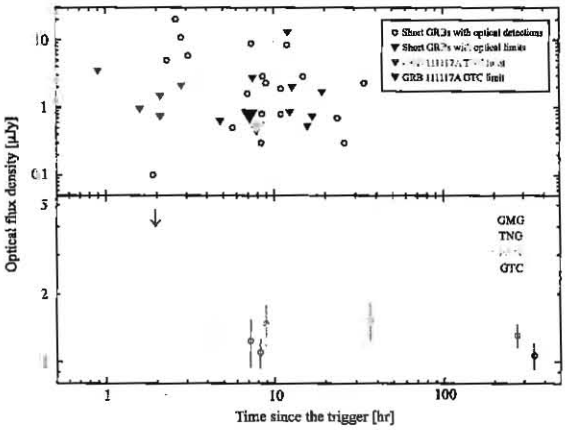

Fig. 6.— Top: optical fluxes of the first optical detection (black circle) or an upper limit (filled triangle) of short GRBs (Berger 2010) is shown as a function of the trigger time. The TNG and GTC upper limits of the optical afterglow of GRB 111117A are shown in green and blue filled triangle. Bottom: optical light curves of GRB 111117A in R and r band are shown. The plot includes R band measurement from GMG, TNG and NOT, and also the r band measurement from GTC.

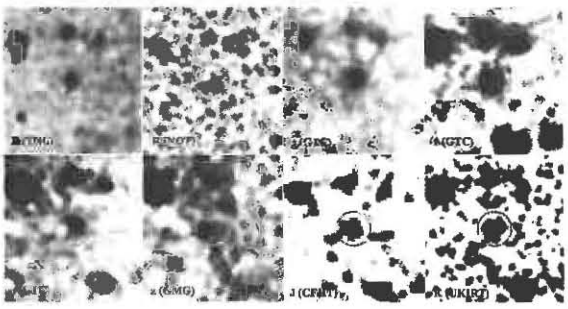

Fig. 7.— Multi-color images at the field of GRB 111117A. From left to right, and top to bottom, the images are TNG R, NOT R, GTC g, GTC r, GTC i, GMG z, CFHT J and UKIRT K. The host galaxy is marked in a green circle. The X-ray afterglow position determined by *Chandra* is marked as a red cross. The image scale is $17'' \times 17''$. All the images are smoothed by the Gaussian function with 3 pixel radius.

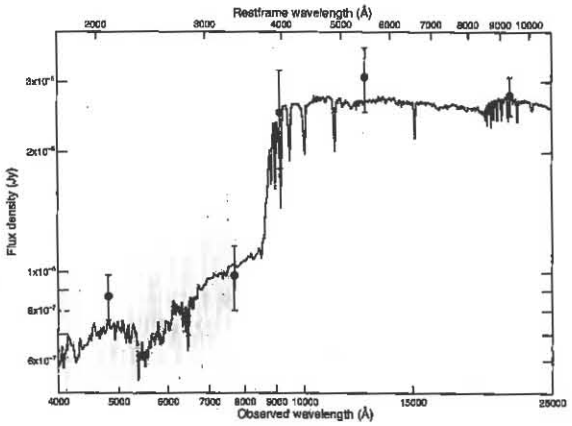

Fig. 8.— The SED fit to the photometric data (g, r, i, z, J and K) using the templates of the single stellar populations model (Maraston 2005). The GTC spectrum is shown in gray.

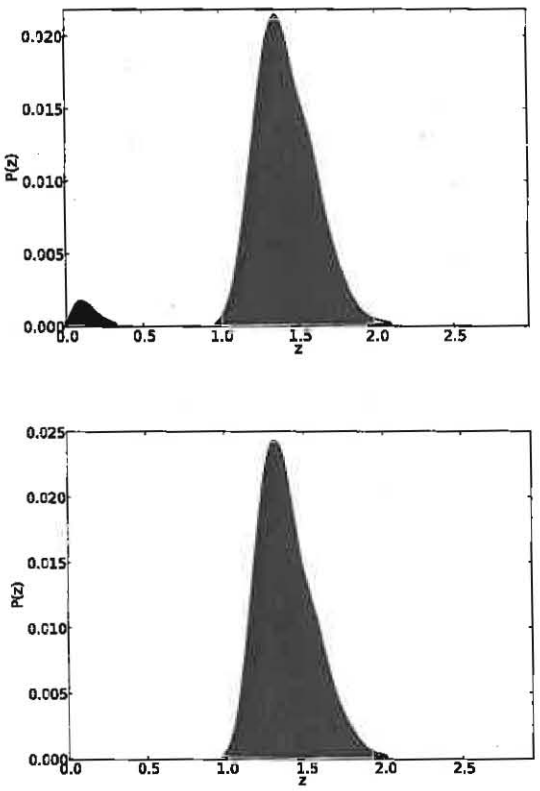

Fig. 9.— Top: Posterior probability distribution of the photometric redshift by the SED fit of the host. All 269 SED templates are used. Bottom: Posterior probability distribution of the photometric redshift of the host by 41 SED templates of a solar metallicity and a red horizontal branch morphology with stellar age from 20 Myr to 15 Gyr.

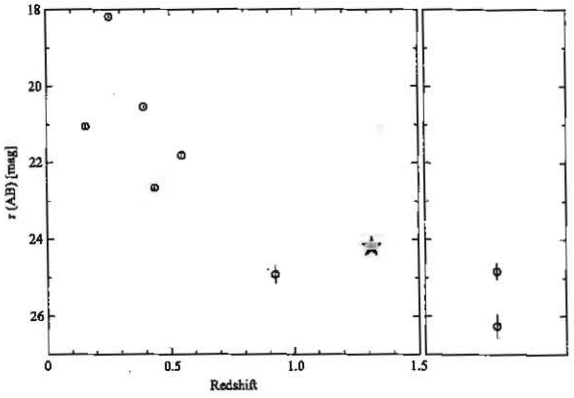

Fig. 10.— Magnitude of the short GRB hosts (from Berger 2010) as a function of redshift. The right panel shows the magnitude of the hosts without a confirmed redshift. GRB 111117A (z=1.31) is shown as a red star.

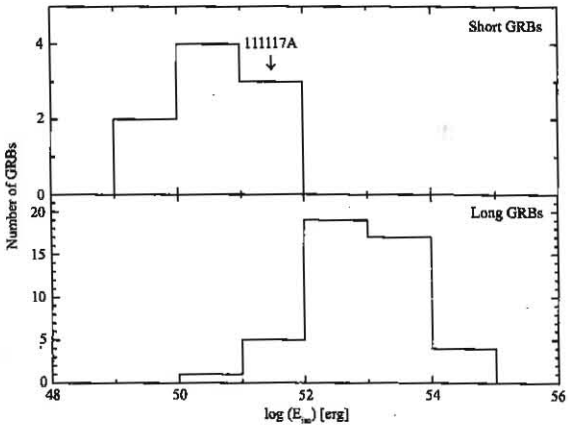

Fig. 11.— Comparison of $E_{\rm iso}$ between short (upper panel) and long (lower panel) GRBs. The short GRB $E_{\rm iso}$ values are from (Berger 2010) (sample1), and the long GRB $E_{\rm iso}$ values are from Nava et al. (2012) (only *Swift* long GRBs). GRB 111117A (3.4×10^{51} erg) is located at the high end of $E_{\rm iso}$ distribution of short GRBs.